

# Epsilon-Neighborhood Decision-Boundary Governed Estimation (EDGE) of 2D black box Classifier Functions <sup>\*</sup>

M. Goutham <sup>\*</sup>, R. DalferroNucci <sup>\*</sup>, S. Stockar <sup>\*</sup>, M. Menon <sup>\*\*</sup>,  
S. Nayak <sup>\*\*</sup>, H. Zade <sup>\*\*</sup>, C. Patel <sup>\*\*</sup>, M. Santillo <sup>\*\*</sup>

<sup>\*</sup> *Department of Mechanical and Aerospace Engineering, The Ohio State University, Columbus, OH 43210 USA (e-mail: goutham.1@osu.edu).*

<sup>\*\*</sup> *Ford Motor Company, Dearborn, MI 48109 USA.*

---

**Abstract:** Accurately estimating decision boundaries in black box systems is critical when ensuring safety, quality, and feasibility in real-world applications. However, existing methods iteratively refine boundary estimates by sampling in regions of uncertainty, without providing guarantees on the closeness to the decision boundary and also result in unnecessary exploration that is especially disadvantageous when evaluations are costly. This paper presents the  $\varepsilon$ -Neighborhood Decision-Boundary Governed Estimation (EDGE), a sample efficient and function-agnostic algorithm that leverages the intermediate value theorem to estimate the location of the decision boundary of a black box binary classifier within a user-specified  $\varepsilon$ -neighborhood. Evaluations are conducted on three nonlinear test functions and a case study of an electric grid stability problem with uncertain renewable power injection. The EDGE algorithm demonstrates superior sample efficiency and better boundary approximation than adaptive sampling techniques and grid-based searches.

*Keywords:* black box systems, Boundary estimation, Classification, Grid Stability

---

## 1. INTRODUCTION

The successful deployment of real-world systems generally relies on satisfying safety, quality, or feasibility criteria, making it essential to precisely characterize how system parameters can vary before resulting in undesirable outcomes (Rogers and Ierapetritou, 2015). This characterization involves identifying the decision boundary that separates “desirable” and “undesirable” system states (Larson and Mattson, 2012). However, in black box systems, explicit expressions describing the system are unavailable, making it impossible to analytically define this boundary, and thus, sampling methods are used (Karimi et al., 2019).

In safety critical applications, it is desirable to guarantee that the estimated boundary is within an  $\varepsilon$ -neighborhood of the true decision boundary, where  $\varepsilon$  is a user-defined parameter that defines the permissible error in localization. Existing black box boundary estimation methods typically refine function approximations by adaptively sampling in regions of high uncertainty to localize the boundary (Ono et al., 2024; Pepper et al., 2022).

Existing methods lack the  $\varepsilon$ -neighborhood guarantee that is necessary to make design and operational decisions that rely on the estimated boundary. Further, these techniques require hyperparameter tuning, demand high computational resources and their performance varies due to underlying randomness (Settles, 2009). Due to the iterative

nature of these methods, points far from the boundary are frequently explored, reducing sample efficiency, which is particularly detrimental when system state evaluations are computationally expensive.

This paper presents the  $\varepsilon$ -Neighborhood Decision-Boundary Governed Estimation (EDGE), a novel algorithm that addresses these challenges in two-dimensional space by:

- (1) Sampling interior and exterior points strictly within a user-defined  $\varepsilon$ -neighborhood of the unknown decision boundary, maximizing sample efficiency
- (2) Spanning the entire boundary with minimal average symmetric surface distance, a metric that quantifies total approximation error with the decision boundary
- (3) Requiring no hyperparameter tuning, making it applicable across various black box system characteristics

After defining the problem and the EDGE algorithm, its effectiveness is demonstrated through a grid stability case study that assesses feasible ranges of power injection from renewable energy sources. Subsequently, the performance of the EDGE algorithm is evaluated using several two-dimensional, highly nonlinear benchmark functions. Its efficiency and accuracy are compared against an active learning method utilizing Support Vector Machines and a naïve  $\varepsilon$ -spaced grid sampling method that provides an  $\varepsilon$ -neighborhood guarantee. Comparatively, the boundary localized by the EDGE algorithm had significantly improved approximation accuracy, sample and computational efficiency.

---

<sup>\*</sup> This research was supported by the Ford Motor Company as part of the Ford-OSU Alliance Program.

## 2. PROBLEM DESCRIPTION

Let  $\mathcal{X} \subseteq \mathbb{R}^2$  be a compact domain of interest. Consider a black box boolean-valued classifier function  $f(\cdot) : \mathcal{X} \rightarrow \mathbb{B}$ . The value  $f(x) = 1$  may imply some desirable property being studied, such as  $x$  being classified as *safe* in some engineering operation, or as *feasible* in a design or optimization problem, or that  $x$  *passes* some defined performance or quality test, etc. The *absence* of the indicated property corresponds to  $f(x) = 0$  in this binary representation.

Let the set  $S^1 := \{x \in \mathcal{X} : f(x) = 1\}$  denote the set of all *interior points* in  $\mathcal{X}$  that are desirable. Denote its complementary set of *exterior points* by  $S^0 := \{x \in \mathcal{X} : f(x) = 0\}$ . The *decision boundary* separating the two sets is given by  $\partial S$  as indicated in Fig. 1a, and corresponds to the interface where  $f(x)$  changes in value.

Defining  $\partial S$  is generally infeasible, especially for a black box function due to a lack of access to its closed-form expression. To overcome this, a tolerance parameter  $\varepsilon$  is introduced to define two bounding sets that capture  $\partial S$ :

The inner  $\varepsilon$ -neighborhood set of  $\partial S$ :

$$\partial S_\varepsilon^1 := \left\{ x \in \mathcal{X} : f(x) = 1, d(x, \partial S) \leq \varepsilon \right\} \quad (1a)$$

The outer  $\varepsilon$ -neighborhood set of  $\partial S$ :

$$\partial S_\varepsilon^0 := \left\{ x \in \mathcal{X} : f(x) = 0, d(x, \partial S) \leq \varepsilon \right\} \quad (1b)$$

In Eq.(1), the distance from a point  $x$  to any point on  $\partial S$  is given by  $d(x, \partial S) := \inf_{y \in \partial S} \|x - y\|$ . The striped regions in Fig.(1) depict  $\partial S_\varepsilon^1$  and  $\partial S_\varepsilon^0$  and comprise the regions in  $\mathcal{X}$  within an  $\varepsilon$ -distance from decision boundary  $\partial S$ , henceforth called the  $\varepsilon$ -neighborhood of  $\partial S$ . The parameter  $\varepsilon$  is chosen based on the desired localization accuracy of the decision boundary — a small  $\varepsilon$ -value indicates a need for a high degree of certainty in the localization of  $\partial S$ .

Despite the  $\varepsilon$ -tolerance, defining  $\partial S_\varepsilon^1$  and  $\partial S_\varepsilon^0$  as per Eqs. (1a) and (1b) remains impossible without explicit knowledge of  $\partial S$ . To address this, we propose a sampling-based approach that constructs inner and outer approximating point sets,  $\partial \tilde{S}^1 \subset \partial S_\varepsilon^1$  and  $\partial \tilde{S}^0 \subset \partial S_\varepsilon^0$ , which bracket the true boundary within its  $\varepsilon$ -neighborhood.

Sample efficiency is an important consideration when attempting to approximate  $\partial S$  through such a sampling-based approach. Minimizing the number of function queries is necessary because queries to  $f(\cdot)$  may be expensive, involving high-fidelity simulations, large-scale combinatorial optimization problems, or physical experiments.

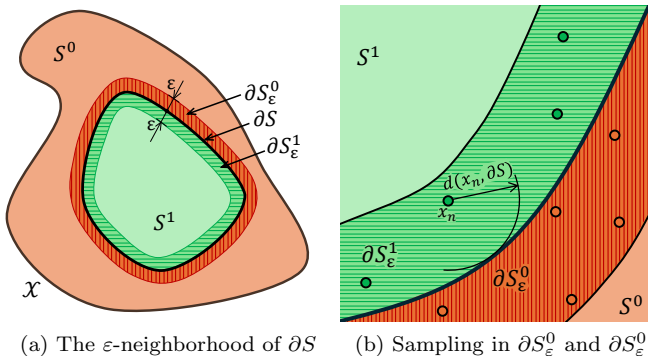


Fig. 1. Definition of sets

The objectives when estimating  $\partial S$  are:

- (1) *Sample Efficiency*: Minimize the number of queries needed to identify points in  $\partial \tilde{S}^0$  and  $\partial \tilde{S}^1$ , thereby approximating  $\partial S$  within its  $\varepsilon$ -neighborhood.
- (2) *Approximation Accuracy*: Minimize the average surface distance (ASD) between the decision boundary  $\partial S$ ,  $\partial \tilde{S}^0$  and  $\partial \tilde{S}^1$  given by:

$$d(\partial \tilde{S}^0, \partial S, \partial \tilde{S}^1) = d(\partial \tilde{S}^0, \partial S) + d(\partial \tilde{S}^1, \partial S) \quad (2a)$$

$$\text{where, } d(\partial \tilde{S}, \partial S) = \frac{1}{|\partial \tilde{S}| + |\partial S|} \left[ \sum_{x \in \partial \tilde{S}} d(x, \partial S) + \sum_{y \in \partial S} d(y, \partial \tilde{S}) \right] \quad (2b)$$

Minimizing  $d(\partial \tilde{S}^0, \partial S, \partial \tilde{S}^1)$  ensures that points in  $\partial \tilde{S}^0$  and  $\partial \tilde{S}^1$  adequately span the boundary  $\partial S$ , avoiding the trivial solution of finding a single point close to  $\partial S$ . Some points of  $\partial \tilde{S}^1$  and  $\partial \tilde{S}^0$  and are shown in illustrative Fig. 1b. Although  $\partial S$  is unknown, for evaluation purposes, it can be closely approximated by choosing a sufficiently low  $\varepsilon$ .

## 3. PROPOSED EDGE ALGORITHM

The intermediate value theorem (IVT) is the key enabler of the EDGE algorithm, ensuring that sampled points lies in the  $\varepsilon$ -neighborhood of  $\partial S$ . If there exist points  $x_n^1$  and  $x_m^0$  satisfying  $f(x_n^1) = 1$  and  $f(x_m^0) = 0$ , and if these points are at a distance  $\|x_n^1 - x_m^0\| \leq \varepsilon$ , then the IVT when applied in the boolean context guarantees that  $\partial S$  intersects the segment connecting  $x_n^1$  and  $x_m^0$ . This means that necessarily, both  $x_n^1 \in \partial \tilde{S}^1$  and  $x_m^0 \in \partial \tilde{S}^0$  because there exists a transition from function value 1 to 0 somewhere along the line segment joining these two points, and therefore,  $d(x_n^1, \partial S) \leq \varepsilon$  and  $d(x_m^0, \partial S) \leq \varepsilon$ .

In practice, a boundary  $\partial S$  need not exist for  $f(\cdot)$  in the domain  $\mathcal{X}$ , but the EDGE algorithm can only be initialized if at least one interior and one exterior point are found. If multiple queries are needed to find these points, denote the closest pair of points as  $\bar{x}_0^{in} \in S^1$  and  $\bar{x}_0^{out} \in S^0$ .

The bisection procedure is first used to localize  $\partial S$  along the segment connecting  $\bar{x}_0^{in}$  and  $\bar{x}_0^{out}$ , as described by Alg. 1. If the midpoint of  $\bar{x}_0^{in}$  and  $\bar{x}_0^{out}$  has a function value of 1, it is appended to the ordered set  $\bar{x}^{in}$  as  $\bar{x}_1^{in}$ . This is as shown in the illustrative example of Fig. 2, repeatedly querying the midpoint of the most recently appended points of sets  $\bar{x}^{in}$  and  $\bar{x}^{out}$ , until the distance between the last appended points of  $\bar{x}_0^{in}$  and  $\bar{x}_0^{out}$  is less than  $\varepsilon$ , thus converging to the  $\varepsilon$ -neighborhood of  $\partial S$ .

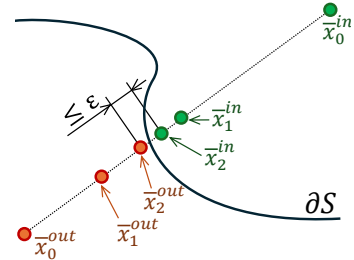


Fig. 2. Bisection to  $\varepsilon$  ball of  $\partial S$

---

**Algorithm 1** Bisection to  $\varepsilon$  ball of  $\partial S$  boundary
 

---

```

1: function BIASECT( $\bar{x}_0^{in}, \bar{x}_0^{out}, \varepsilon$ )
2:    $\bar{x}^{in} \leftarrow \bar{x}_0^{in}; \bar{x}^{out} \leftarrow \bar{x}_0^{out}$ 
3:   while  $\|\bar{x}_{end}^{in} - \bar{x}_{end}^{out}\| \geq \varepsilon$  do
4:      $x_{test} \leftarrow (\bar{x}_{end}^{in} + \bar{x}_{end}^{out})/2$ 
5:     if  $f(x_{test}) = 0$  then  $\triangleright$  Exterior test point
6:       Append  $x_{test}$  to  $\bar{x}^{out}$ 
7:     else  $\triangleright$  Interior test point
8:       Append  $x_{test}$  to  $\bar{x}^{in}$ 
9:     end if
10:  end while
11:  return  $\bar{x}^{in}, \bar{x}^{out}$ 
12: end function

```

---

The last appended points of the interior bisection sequences  $\bar{x}_{end}^{in}$  and  $\bar{x}_{end}^{out}$  are the first points  $\partial\tilde{S}_0^1$  and  $\partial\tilde{S}_0^0$  of the inner and outer point sets respectively. These points initiate the decision boundary walk of Alg. 2.

Let  $\text{circle}(x_c, \varepsilon)$  represent the  $\varepsilon$ -radius circle centered at  $x_c$ , or equivalently, the set  $\{x : \|x - x_c\| = \varepsilon\}$ . As shown in Fig. 3, the intersection of  $\text{circle}(\partial\tilde{S}_0^1, \varepsilon)$  and  $\text{circle}(\partial\tilde{S}_0^0, \varepsilon)$  is first obtained. This produces two intersection points that form set  $C$  of line 4 in Alg. 2. The intersection point which has a positive cross product relative to the points  $\partial\tilde{S}_0^1$  and  $\partial\tilde{S}_0^0$  is selected as  $x_{test}$ , per line 5 of Alg. 2.

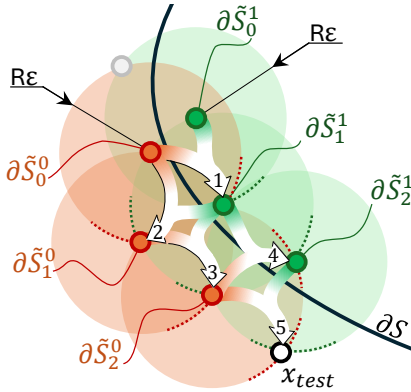


Fig. 3.  $\varepsilon$ -stepping along  $\partial S$  boundary

---

**Algorithm 2** Decision Boundary Walk
 

---

```

1: function DECISIONBOUNDARY( $\bar{x}^{in}, \bar{x}^{out}, \partial\mathcal{X}, \varepsilon$ )
2:    $\partial\tilde{S}^1 \leftarrow \bar{x}^{in}; \partial\tilde{S}^0 \leftarrow \bar{x}^{out}$ 
3:   repeat
4:      $C \leftarrow \{\text{circle}(\partial\tilde{S}_{end}^1, \varepsilon) \cap \text{circle}(\partial\tilde{S}_{end}^0, \varepsilon)\}$ 
5:      $x_{test} \leftarrow x \in C | (\partial\tilde{S}_{end}^0 - \partial\tilde{S}_{end}^1) \times (x - \partial\tilde{S}_{end}^1) > 0$ 
6:     if  $x_{test} \in \mathcal{X}$  then
7:       if  $f(x_{test}) = 0$  then  $\triangleright$  Exterior test point
8:         Append  $x_{test}$  to  $\bar{x}^{out}$ 
9:       else  $\triangleright$  Interior test point
10:        Append  $x_{test}$  to  $\bar{x}^{in}$ 
11:      end if
12:    else
13:      DOMAINBOUNDARY( $\partial\tilde{S}^1, \partial\tilde{S}^0, \partial\mathcal{X}, \varepsilon$ )
14:    end if
15:  until  $\min\{\|x_{test} - \partial\tilde{S}_0^1\|, \|x_{test} - \partial\tilde{S}_0^0\|\} \leq \varepsilon$ 
16:    and  $\min\{|\partial\tilde{S}^1|, |\partial\tilde{S}^0|\} > 1$ 
17:  return  $\partial\tilde{S}^1, \partial\tilde{S}^0$ 
18: end function

```

---

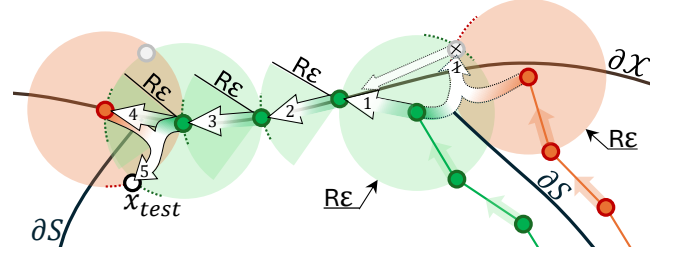


Fig. 4.  $\varepsilon$ -stepping along  $\partial\mathcal{X}$  boundary

---

**Algorithm 3** Domain Boundary Walk
 

---

```

1: function DOMAINBOUNDARY( $\partial\tilde{S}^1, \partial\tilde{S}^0, \partial\mathcal{X}, \varepsilon$ )
2:    $\{x_1, x_2\} \leftarrow \{x \in \partial\mathcal{X} \mid \|x - \partial\tilde{S}_{end}^1\| = \varepsilon\}$ 
3:    $x_{test} \leftarrow \arg \max_{x \in \{x_1, x_2\}} \|x - \partial\tilde{S}_{end}^0\|$ 
4:   while  $f(x_{test}) = 1$  do
5:     Append  $x_{test}$  to  $\partial\tilde{S}^1$ 
6:      $x_{test} \leftarrow \{x \in \partial\mathcal{X} \setminus \partial\tilde{S}^1 \mid \|x - \partial\tilde{S}_{end}^1\| = \varepsilon\}$ 
7:   end while
8:   Append  $x_{test}$  to  $\partial\tilde{S}^0$ 
9:   return  $\partial\tilde{S}^1, \partial\tilde{S}^0$ 
10: end function

```

---

The selection of a positive cross product is arbitrary, and could instead be negative, so long as the direction sense is maintained throughout Alg. 2. In the illustrative example of Fig. 3, the first  $x_{test}$  point returned  $f(x_{test}) = 1$ , and is appended as  $\partial\tilde{S}_1^1$  of inner set  $\partial\tilde{S}^1$ . Next, the intersection points of  $\text{circle}(\partial\tilde{S}_1^1, \varepsilon)$  and  $\text{circle}(\partial\tilde{S}_0^0, \varepsilon)$ , the last point of the  $\tilde{S}^0$  set are obtained. The point that satisfies a positive relative cross product is queried, and appended to the appropriate set. In this manner, Alg. 2 repeatedly steps by an  $\varepsilon$  distance along both sides of  $\partial S$  in its  $\varepsilon$ -neighborhood.

If a test point  $x_{test}$  is found to be outside the domain  $\mathcal{X}$ , an  $\varepsilon$ -stepping walk is conducted along  $\partial\mathcal{X}$ , as detailed in Alg. 3 and illustrated by Fig. 4. First, two candidate points  $x_1, x_2$  on  $\partial\mathcal{X}$  are identified that are  $\varepsilon$  away from the  $\partial\tilde{S}_{end}^1$  point. As defined in step 3 of Alg. 3, the point farther away from the  $\partial\tilde{S}_{end}^0$  point is selected as  $x_{test}$ . This preference ensures that the boundary intersecting  $\partial\mathcal{X}$  is identified.

The while-loop of steps 4-7 continues to select test points along  $\partial\mathcal{X}$  in the same direction sense, appending encountered interior points to  $\partial\tilde{S}^1$ . This is executed until an exterior point is detected, which is appended to  $\partial\tilde{S}^0$ , and indicates that  $\partial S$  has been detected, re-initiating Alg. 2.

The decision boundary walk of Alg. 2 is continued until a test point is within an  $\varepsilon$  distance away from one of the initializing points  $\partial\tilde{S}_0^1$  or  $\partial\tilde{S}_0^0$ . This indicates that the entire length of  $\partial S \in \mathcal{X}$  has been spanned within an  $\varepsilon$ -tolerance and the EDGE algorithm is terminated, returning the  $\partial\tilde{S}^1$  and  $\partial\tilde{S}^0$  sets, that is, the inner and outer approximation sets of  $\partial S \in \mathcal{X}$ .

The EDGE algorithm is function agnostic since it has no hyper-parameters that require tuning, and can be applied to any black box function. While the bisection algorithm produces unavoidable function queries in regions outside  $\partial\tilde{S}^1$  and  $\partial\tilde{S}^0$ , the  $\varepsilon$ -stepping algorithms for the decision and domain boundaries yield a 100% sample efficiency, that is, every sampled point is appended to  $\partial\tilde{S}^1$  or  $\partial\tilde{S}^0$ .

## 4. COMPUTATIONAL EXPERIMENTS

### 4.1 Case Study: Power Grid with Renewable Sources

Consider a power grid network represented by a set of buses  $i \in \mathcal{B}$ , generators  $g \in \mathcal{G}$  and transmission lines  $ij \in \mathcal{L}$ . The DC Optimal Power Flow (DC OPF) formulation is a grid model commonly used for stability analysis, enabling real-time response to varying demands & renewable power generation (Bynum et al., 2021; Purchala et al., 2005). The minimization problem of Eq. (3) determines the most economical operating point for a power grid, where  $c_g$  is the operational cost associated with generator  $g$  and  $p_g$  is its power output:

$$J = \min \sum_{g \in \mathcal{G}} c_g p_g \quad (3a)$$

$$\text{s.t.} \quad \sum_{g \in \mathcal{G}_i} p_g + \sum_{j \in \mathcal{L}} p_{ji} = \sum_{d \in \mathcal{D}_i} p_d, \quad \forall i \in \mathcal{B} \quad (3b)$$

$$p_g \leq p_g \leq \bar{p}_g, \quad \forall g \in \mathcal{G} \quad (3c)$$

$$-\bar{p}_{ij} \leq p_{ij} \leq \bar{p}_{ij}, \quad \forall ij \in \mathcal{L} \quad (3d)$$

$$p_{ij} = -b_{ij}(\theta_i - \theta_j), \quad \forall ij \in \mathcal{L} \quad (3e)$$

$$\underline{\theta}_{ij} \leq \theta_i - \theta_j \leq \bar{\theta}_{ij}, \quad \forall ij \in \mathcal{L} \quad (3f)$$

The constraints defined by Eq. (3b) - (3f) capture grid power flow physics. Nodal power balance at each bus  $i \in \mathcal{B}$  is imposed by Eq. (3b), ensuring that the sum of the power produced by all generators  $\sum_{g \in \mathcal{G}_i} p_g$  co-located at bus  $i$  and the net incoming power flow  $\sum_{j \in \mathcal{L}} p_{ji}$  through transmission lines equals the total load demanded  $\sum_{d \in \mathcal{D}_i} p_d$  at bus  $i$ . Each generator  $g \in \mathcal{G}$  is constrained by Eq. (3c) to operate within its minimum and maximum power limits of  $p_g$  and  $\bar{p}_g$  respectively. Similarly, transmission line flow constraints of Eq. (3d) ensure that the power flow  $p_{ij}$  on any line  $ij \in \mathcal{L}$  does not exceed the specified maximum flow  $\bar{p}_{ij}$  in either direction. The DC power flow relationship is defined in Eq. (3e) using line susceptance  $b_{ij}$  and the difference in voltage phase angles  $\theta_i$  and  $\theta_j$  to determine the flow on each line  $p_{ij}$ . Finally, Eq. (3f) enforces the limits  $\underline{\theta}_{ij}$  and  $\bar{\theta}_{ij}$  on the permissible phase angle differences between connected buses  $i, j$ .

When renewable resources such as solar arrays or wind farms are connected to the grid, their power output is governed by changing environmental factors. Because these sources cannot be directly controlled like conventional power generators, their power output appears as system parameters that vary as a function of incident solar irradiance or wind speed. The varying renewable power injection can disrupt nodal power balance or cause violations of generator, line flow, or phase angle constraints defined by Eq. (3b) - (3f). Consequently, careful selection of power ratings of these renewable sources is essential to maintain stable operation despite their inherent variability.

This case study uses the widely used IEEE 5-bus system and its defined parameters (Li and Bo, 2010). Generators 1 and 5 are replaced by renewable power sources rated at 10 and 7 MW, respectively. The domain  $\mathcal{X}$  is therefore defined as  $[0, 10] \times [0, 7]$ , reflecting the expected variation in power output for these two generators.

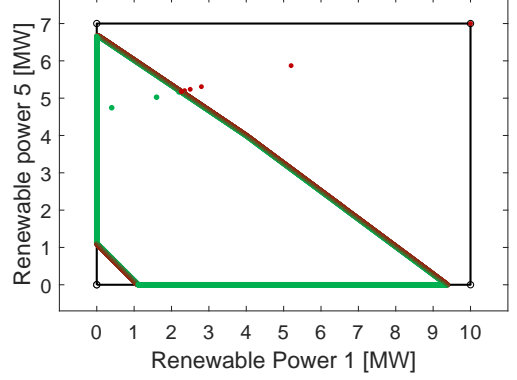


Fig. 5. Power injection  $\partial S$  ( $\varepsilon = 0.01 MW$ )

The first interior point,  $\bar{x}_0^{in}$ , is selected as the nominal grid operating state prior to the integration of renewable sources, marked in green at the coordinate (0.4, 4.74) in Fig. 5. To identify an exterior point, the four corner points are then evaluated. In this case, the first corner inspected, (10, 7) is confirmed to be  $\bar{x}_0^{out}$ , an exterior point because it violated one of the constraints defined in Eqs. (3b)–(3f).

The bisection algorithm is initiated with  $\bar{x}_0^{in}$  and  $\bar{x}_0^{out}$ , converging to the specified  $\varepsilon$ -neighborhood, after which the  $\varepsilon$ -stepping algorithms are used to span  $\partial S \in \mathcal{X}$ . When the  $\varepsilon$  value was set to 0.01 MW, the true boundary was delineated by sampling 2,866 points, while an  $\varepsilon$  value of 0.1 MW required 282 points.

This illustrative example treated the DC-OPF feasibility problem as a black box classifier  $f(\cdot)$ , i.e., it remained inaccessible to the EDGE algorithm. Despite this, the resulting approximated boundary is clearly a polygon, as expected for this linear formulation. Although a linear formulation was used here, the EDGE algorithm can be applied without any tuning to data-driven grid models or nonlinear formulations capturing cascading and transient effects in larger grid systems.

### 4.2 Nonlinear Test Functions

For the following test cases, the boundary  $\partial S$  corresponds to the level set where a 2D test function attains a specified constant value. For the Rosenbrock test function defined by Eq. (4a), the domain is given by  $\mathcal{X}_f := [-6, 6] \times [-2, 10]$ , and  $\partial S$  is defined by  $f(x, y) = 100$ . Interior points satisfy  $f(x, y) < 100$  and exterior points satisfy  $f(x, y) > 100$ .

$$f(x, y) = (1 - x)^2 + 100(y - x^2)^2 \quad (4a)$$

$$g(x, y) = [1 + (x + y + 1)^2 \times (19 - 14x + 3x^2 - 14y + 6xy + 3y^2)] \times [30 + (2x - 3y)^2 \times (18 - 32x + 12x^2 + 48y - 36xy + 27y^2)] \quad (4b)$$

$$h(x, y) = (1.5 - x + xy)^2 + (2.25 - x + xy^2)^2 + (2.625 - x + xy^3)^2 \quad (4c)$$

The Goldenstein-Price and Beale test functions defined by Eq. (4b) and (4c) are similarly binarized, setting  $g(x, y) = 100$  and  $f(x, y) = 3e5$  to define decision boundaries. Their domains are defined by  $\mathcal{X}_g := [-8, 10] \times [-7, 6]$  and  $\mathcal{X}_h := [-6, 6] \times [-7, 7]$  respectively.

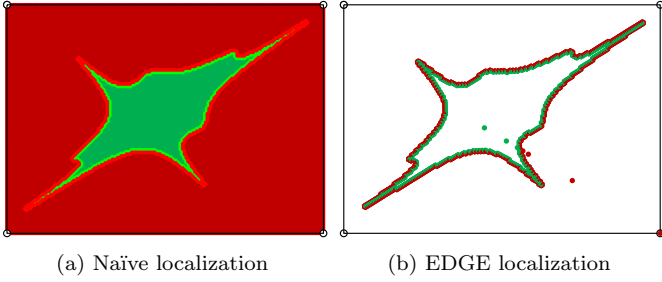


Fig. 6. Goldenstein-Price test function  $g(x, y) = 100$

#### 4.3 Benchmark Alg. 1: Naïve Grid Sampling

Due to a lack of methods in literature that localize  $\partial S$  to within its  $\varepsilon$ -neighborhood, in this paper, a simple algorithm is developed as a benchmark that meets the objective. This naïve approach samples  $\mathcal{X}$  on a uniform grid of  $\varepsilon$ -spaced points, querying each grid point to identify if a point belongs to  $S^1$  or  $S^0$ . Once every grid point has been classified, point labels are inspected in each  $\varepsilon$ -neighborhood, detecting  $\partial\tilde{S}^0$  and  $\partial\tilde{S}^1$  points based on the encountered label transitions. This guarantees  $\varepsilon$ -neighborhood localization of  $\partial S$  while also spanning the entire boundary, minimizing ASD, i.e.,  $d(\partial\tilde{S}^0, \partial S, \partial\tilde{S}^1)$ .

As shown in Fig. 6a, this approach tests every point in the grid, localizing  $\partial S$  within its  $\varepsilon$ -neighborhood. Compared with the EDGE algorithm, whose sampled points are shown in Fig. 6b, the naïve approach has poor sample efficiency and is computationally prohibitive for large domains. Table 1 lists outcomes for the 3 test functions.

#### 4.4 Benchmark Alg. 2: Active Learning at the Boundaries

The performance of the EDGE algorithm is also compared with an active learning at the boundaries (ALB) algorithm which uses an iterative Support Vector Machine (SVM) approach (Kremer et al., 2014). SVM is a supervised machine learning method that seeks to identify the decision boundary that separates two labeled sets of data points with the largest possible margin (Vapnik, 1995).

SVMs use kernel functions  $k(x_i, x_j)$  to quantify the correlation between labels at points  $x_i$  and  $x_j$ . In black box applications, the Radial Basis Function (RBF) kernel is typically chosen (AlBahar et al., 2021). This kernel is defined by  $k(x_i, x_j) = \exp(-\|x_i - x_j\|^2/2\sigma^2)$ , where  $\sigma$  is a width hyperparameter that determines the influence of one training example on the predicted decision boundaries.

The active learning component iteratively samples from regions of high uncertainty, i.e., the predicted decision boundary region. It executes the following:

- (1) Randomly generate  $n_{init}$  unlabeled points in  $\mathcal{X}$
- (2) Label them using  $f(\cdot) : \mathcal{X} \rightarrow \{0, 1\}$
- (3) Train SVM using labeled set available
- (4) Identify  $n_{learn}$  points at the predicted boundary
- (5) Repeat steps 2 to 4 until budget is exhausted

In this study, the SVM was implemented within MATLAB's SVM solver *fitcsvm*, with default RBF parameters. The hyperparameters  $n_{init}$  and  $n_{learn}$  were set to 100 and 30 respectively by tuning for time and sample efficiency for the 3 test functions of (4).

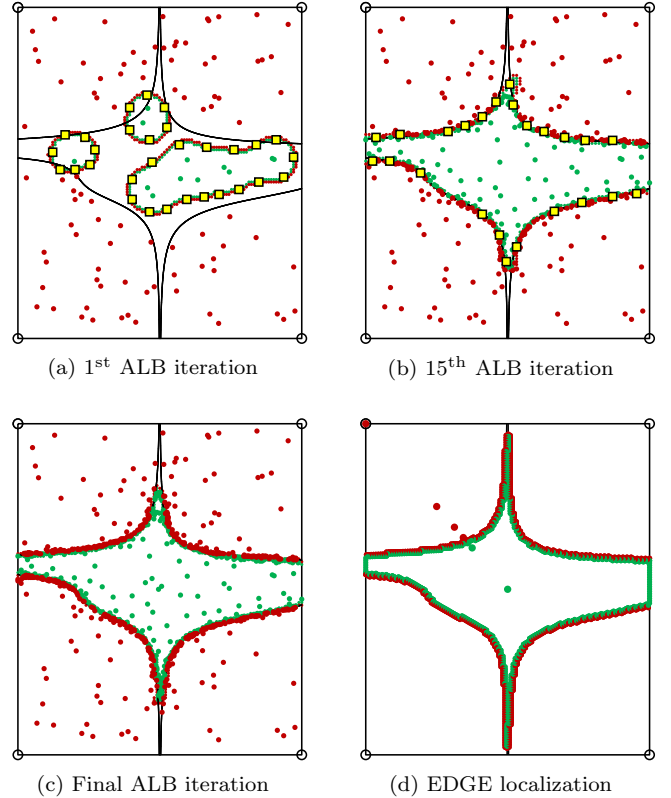


Fig. 7. Beale Test Function

As illustrated using the Beale test function  $h(x, y)$  in Fig. 7a,  $n_{init}$  points are first randomly sampled in the domain  $\mathcal{X}$  and then labeled. In this example, the SVM predicts three disjoint boundaries as shown, obtained by training on the  $n_{init}$  randomly sampled points. The true boundary  $\partial S$  is shown by the black contour, and the ALB's objective is to iteratively select points for labeling to improve the  $\partial S$  localization accuracy of the predicted boundary.

For the next iteration, sufficiently well-spaced points, marked by yellow squares in Fig. 7a, are selected at these boundaries to be queried by  $h(x, y)$ . These points are selected by  $k$ -means clustering on the predicted boundary to define  $n_{learn}$  clusters, after which the predicted boundary point closest to the centroid of each cluster is chosen. These newly labeled points are added to the training set, and the process is repeated. As seen in Fig. 7b, after 15 iterations, the predicted boundary better approximates  $\partial S$ .

For comparative evaluation, the sample budget of the ALB algorithm is limited to the number of samples used by the EDGE algorithm. The resulting ALB-localized boundary shown in Fig. 7c does not capture the nonlinear regions of  $\partial S$  as closely as the EDGE boundary of Fig. 7d.

All experiments were conducted in a Matlab R2023b environment using an AMD Ryzen 5 5600X CPU clocked at 3.7 GHz, equipped with 128 GB RAM. To account for stochasticity associated with the initialization through random points, the ALB algorithm is repeated 30 times. For the Rosenbrock test function, the convergence of ALB's accuracy as a ratio of its ASD with that of EDGE is plotted in Fig. 8. For  $\varepsilon$  values of 0.1 and 0.05, the ASD accuracy, sample efficiency and computation time are noted for the 3 test functions and 3 algorithms in Table 1.

Table 1. Comparison of three optimization methods

Test Function	$\varepsilon$	ASD			Sample Count			Computation Time [s]		
		EDGE	ALB $\mu(\sigma)$	Grid	EDGE	ALB	Grid	EDGE	ALB $\mu(\sigma)$	Grid
Rosenbrock	0.1	0.103	0.845 (0.665)	0.112	973	←	14641	0.08	44.7 (14.060)	0.60
	0.05	0.052	0.600 (0.520)	0.051	1948	←	58081	0.13	1378.23 (356.82)	6.69
Goldenstein-Price	0.1	0.112	0.661 (0.247)	0.111	1101	←	23711	0.06	54.11 (16.62)	1.15
	0.05	0.052	0.530 (0.170)	0.051	2262	←	94221	0.14	1184.40 (207.62)	21.22
Beale	0.1	0.116	0.515 (0.150)	0.112	909	←	17061	0.07	18.07 (3.09)	0.69
	0.05	0.055	0.374 (0.123)	0.054	1903	←	67721	0.13	764.52 (175.59)	7.88

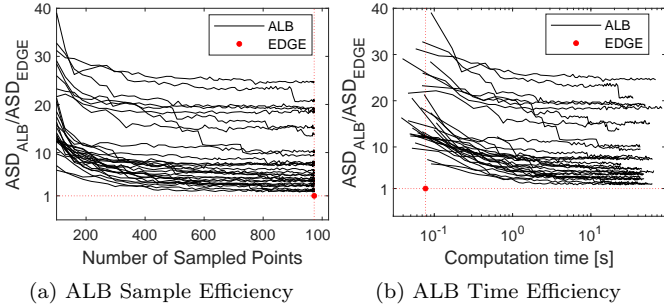


Fig. 8. Rosenbrock Test Function ( $\varepsilon = 0.05$ )

## 5. DISCUSSION

While the ALB algorithm reduces its approximation error, i.e., ASD, by iteratively refining its localization of  $\partial S$ , its performance is influenced by the  $n_{init}$  initialization points, as evident in the significant stochasticity seen in Fig. 8 and listed in Table 1. Contrarily, the EDGE algorithm shows no stochasticity, had lower ASD values across ALB repetitions, test functions, and  $\varepsilon$  values. The ALB method also required higher computation time due to SVM’s time complexity of  $\mathcal{O}(m^3)$  due to kernel matrix computations.

The  $\varepsilon$ -neighborhood guarantee is absent in the ALB, but is provided by both the EDGE algorithm and the naïve grid-search method. As seen in Table 1 however, the sample efficiency of the EDGE algorithm is vastly superior to the uniform grid-search method while providing similar ASD values. The naïve grid-search method also scales poorly because the sample count over a rectangular domain of sides  $a, b$  is given by  $ab/\varepsilon^2$ , and thus, for the same  $\partial S$  perimeter, if the lengths  $a, b$  are doubled or  $\varepsilon$  is halved, the number of naïve approach queries is quadrupled.

## 6. CONCLUSION

The proposed EDGE algorithm leverages the intermediate value theorem to approximate the decision boundary using greedy geometric operations. EDGE outperforms existing active learning approaches in both boundary approximation accuracy and computational efficiency. Unlike active learning methods, EDGE guarantees that its boundary estimation is within the  $\varepsilon$ -neighborhood of the true boundary. EDGE also does not require any hyperparameter tuning, enabling its application to diverse black-box systems.

Future work will focus on expanding the capabilities of EDGE to higher dimensions and extending the binary framework to multiclass problems by decomposition into multiple binary classification problems. The framework can also be extended to stochastic black box systems with system or measurement noise, since the the parameter  $\varepsilon$

offers a soft transition zone between regions. Further, the boundary points identified by EDGE are SVM support vectors, and thus, training SVMs using the labeled point sets of EDGE will boost sample efficiency by prioritizing exploration in transition zones that contribute to SVM performance. Adaptive  $\varepsilon$  stepping will also improve sample efficiency by obtaining coarse approximations of the boundary before localizing to the user defined tolerance.

## REFERENCES

- AlBahar, A., Kim, I., and Yue, X. (2021). A robust asymmetric kernel function for bayesian optimization, with application to image defect detection in manufacturing systems. *IEEE Transactions on Automation Science and Engineering*, 19(4), 3222–3233.
- Bynum, M., Staid, a., Arguello, B., Castillo, A., Knueven, B., Laird, C.D., and Watson, J.P. (2021). Proactive operations and investment planning via stochastic optimization to enhance power systems’ extreme weather resilience. *Journal of Infrastructure Systems*, 27(Sand2021-1171J).
- Karimi, H., Derr, T., and Tang, J. (2019). Characterizing the decision boundary of deep neural networks. *arXiv preprint arXiv:1912.11460*.
- Kremer, J., Steenstrup Pedersen, K., and Igel, C. (2014). Active learning with support vector machines. *Wiley Interdisciplinary Reviews: Data Mining and Knowledge Discovery*, 4(4), 313–326.
- Larson, B.J. and Mattson, C.A. (2012). Design space exploration for quantifying a system model’s feasible domain. *Journal of Mechanical Design*, 134(4), 041010. doi:10.1115/1.4005861. URL <https://doi.org/10.1115/1.4005861>.
- Li, F. and Bo, R. (2010). Small test systems for power system economic studies. In *IEEE PES general meeting*, 1–4.
- Ono, Y., Aczel, T., Estermann, B., and Wattenhofer, R. (2024). Supclust: Active learning at the boundaries. *arXiv preprint arXiv:2403.03741*.
- Pepper, N., Crespo, L., and Montomoli, F. (2022). Adaptive learning for reliability analysis using support vector machines. *Reliability Engineering and System Safety*, 226, 108635.
- Purchala, K., Meeus, L., Van Dommelen, D., and Belmans, R. (2005). Usefulness of DC power flow for active power flow analysis. In *IEEE PES general meeting*, 454–459.
- Rogers, A. and Ierapetritou, M. (2015). Feasibility and flexibility analysis of black-box processes part 1: Surrogate-based feasibility analysis. *Chemical Engineering Science*, 137, 986–1004.
- Settles, B. (2009). Active learning literature survey.
- Vapnik, V. (1995). Support-vector networks. *Machine learning*, 20, 273–297.